Available online at www.sciencedirect.com
SCIENCE DIRECT®
Biochemical and Biophysical Research Communications 318 (2004) 73–80
BBRC
www.elsevier.com/locate/ybbrc

Cu^+ distribution in metallothionein fragments

Maria T. Salgado and Martin J. Stillman*

Department of Chemistry, University of Western Ontario, London, Ont., Canada N6A 5B7

Received 18 March 2004

Abstract

The differential distribution of Cu^+ between separate α and β domains of metallothionein (the isolated peptide fragments) and the rate of transfer of Cu^+ between the two domains using copper–thiolate specific emission spectroscopy are reported. Kinetic data show the rate of transfer of Cu^+ from the $Cu_6\alpha$ to the $Cd_3\beta$ domain is $2 \times 10^{-1}\ s^{-1}$ while the transfer from $Cu_6\beta$ to the $Cd_4\alpha$ domain is much slower at $8 \times 10^{-3}\ s^{-1}$, indicating the greater binding affinity of Cu^+ for the MT β domain. We report that the emission intensity of $Cu_6\beta$ is 0.45 the emission intensity of $Cu_6\alpha$–MT. λ_{max} is shown to be a probe of the environment of the Cu^+. A series of copper-containing domain intermediates to the formation of the filled Cu_6S_9-β and Cu_6S_{11}-α-clusters are identified. A mechanism is proposed for the formation of $Cu_{12}(\beta\alpha)$–MT that involves metal exchange reactions of Cu^+ ions from the α to the β domain with initial formation of a $Cu_4\beta$-cluster.

Keywords: Emission spectroscopy; Copper–thiolate clusters; α and β domains; Metallothionein; Copper transport; Kinetic analysis

Copper is an essential trace element required for the normal growth and development of all organisms, however, excess concentrations of copper can become harmful [1] when not bound to appropriate biological chelators [1,2]. Copper–metallothionein (Cu–MT) has been proposed as one of the major metal-transport systems that newly synthesized proteins use as their source of copper [3]. Metallothioneins (MT) are a unique class of low molecular weight metalloproteins found in vertebrates, invertebrates, fungi, and yeast, characterized by a high cysteine content and an absence of both aromatic residues and disulfide bonds [4]. Exposure of an organism to Zn^{2+}, Cu^+, Cd^{2+}, and Hg^{2+} ions results in induction at the transcriptional level of rapid de novo synthesis of metallothionein, to which these metals bind [5–9]. Binding of copper to MT serves as a protective role by suppressing copper toxicity because Cu–MT decreases the ability of the metal ions to participate in harmful intracellular interactions [2], and so MT has been linked to play a key role in the storage, transport or detoxification of essential and nonessential metal ions [2,4]. Therefore, it is of great importance to understand the mechanisms by which MT sequesters and transfers metals such as Cu^+, due to the wide range of copper-dependent proteins present in biological systems that play a crucial part in the proper functioning of biological systems [1–3].

Metal binding in mammalian MT takes place through metal–thiolate bonds that cross-link the protein into its final three-dimensional structure that involves two distinctive metal–thiolate clusters [2–10], the N-terminal, β domain and the C-terminal, α domain. The three-dimensional structure depends on the metal identity, coordination preference, and number of metals bound to the protein. Seven divalent Cd^{2+} metal ions bind with tetrahedral coordination geometry to MT, whereas, monovalent Cu^+ metal ions bind with trigonal or diagonal coordination with the cysteine sulfurs of the protein and exhibit saturation up to 12 metals [2,4]. Fig. 1 shows the binding stoichiometry and cluster arrangement in mammalian MT for both tetrahedral Cd^{2+} (CdS_4) and trigonal Cu^+ (CuS_3) metal ions [11], creating domain stoichiometries of Cd_3S_9-β and Cd_4S_{11}-α [10,12,13] for Cd^{2+} ions and Cu_6S_9-β and Cu_6S_{11}-α for Cu^+ ions [11,14]. The conformational differences imparted by these two metals are significant and the metal-dependent, three-dimensional structure may be a key

* Corresponding author. Fax: +1-519-661-3022.
E-mail address: Martin.Stillman@uwo.ca (M.J. Stillman).

0006-291X/$ - see front matter © 2004 Elsevier Inc. All rights reserved.
doi:10.1016/j.bbrc.2004.03.183

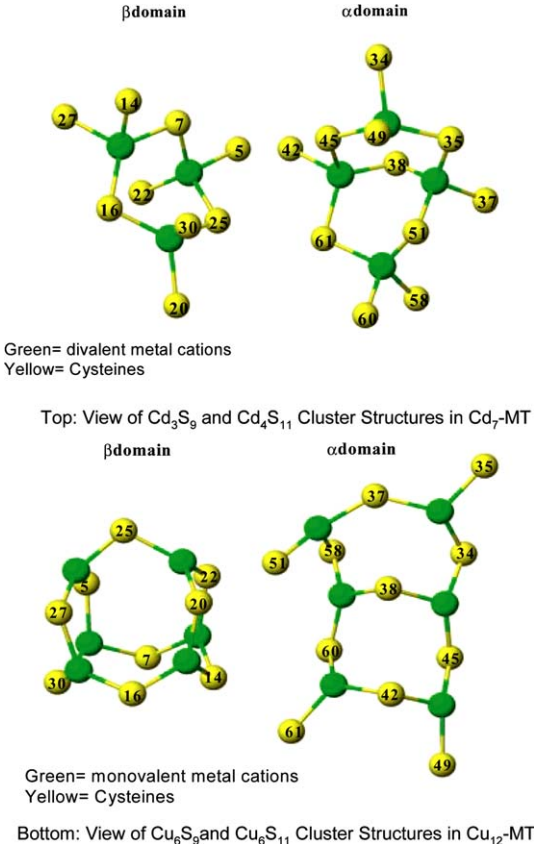

Fig. 1. Ball-and-stick metal connectivity models for (top) the Cd^{2+}–thiolate clusters in each domain of rabbit liver Cd_7–MT, based on NMR connectivities [10,13] and (bottom): the Cu^+–thiolate clusters in each domain of rabbit liver Cu_{12}–MT, based on calculations of Presta et al. [11].

characteristic by which cells are able to discriminate between different metallated forms of MT [15].

The copper binding properties of mammalian MT have been studied widely by a number of authors using primarily NMR, CD, absorption, and emission spectroscopy [14,16–25], recently, studies have focused on the domain specificity of MT for this metal ion [26–28]. This paper provides answers to questions that still remain concerning the mechanism of Cu^+ binding to zinc- or cadmium-containing metallothioneins [26–34], by proposing a copper binding mechanism that is β domain specific when both α and β domains were present at neutral pH under conditions of low copper concentrations.

We take advantage of the specific copper–thiolate optical emissive properties of Cu-substituted α and β domains of MT to detect the preferential binding of Cu^+ to the β domain of MT as a function of time and we use emission properties of Cu–MT (intensity and band maxima, λ_{max}) to determine the stoichiometric distribution of Cu^+ ions between the α and β domains of MT as a function of time. The binding properties of each isolated domain are correlated to the behavior of the two-domain protein, leading to a proposal of a unique pathway for the formation of Cu_6S_9-β and Cu_6S_{11}-α-clusters in MT.

Materials and methods

Recombinant Cd_4α–MT and Cd_3β–MT fragments were produced, isolated, and purified from overexpression in *Escherichia coli* cells [35]. Aqueous protein solutions were prepared in argon-saturated, deionized water, and kept at neutral pH. Protein concentrations were determined by measuring cadmium concentrations using atomic absorption spectroscopy (AAS; Varian AA-875 series) and by determining the concentration of the -SH groups by DTNB (5,5-dithiobis(-2 nitrobenzoic acid)) in the presence of 6 M guanidine hydrochloride [36]. Cu^+ solutions were prepared by dissolving $[Cu(CH_3CN)_4]PF_6$ in a 30% (v/v) argon-saturated acetonitrile/water solution to a final Cu^+ concentration of 5 mM, as determined by AAS. Emission data were recorded on a Photon Technology Quanta Master (QM4/2003) scanning spectrofluorometer. Steady state emission experiments in the region 400–800 nm using a 290 nm excitation wavelength were analyzed by monitoring the changes in λ_{max} and emission intensity near 600 nm as a function of copper loading and time. Schott BG-24 and Schott GG-420 optical glass filters were used to reduce stray light.

Emission intensities and λ_{max} values were obtained by fitting steady state emission spectra with a special deconvoluting program, Simpfit, that provides quantitative estimates of the band center, band width, and band intensity [37]. Determination of the stoichiometry in the $Cd_mCu_n\alpha$, and $Cd_mCu_n\beta$ species formed in the mixing experiments was carried out by simulating the experimental data with the parameters extracted from the individual $Cu_n\alpha$ and $Cu_n\beta$ data sets (which had specific emission intensity and λ_{max} values).

Results and discussion

Emission intensity as a function of copper loading in the isolated α and β domains of MT

The emission intensity near 600 nm was recorded as a function of copper loading for μL aliquots of Cu^+ to 10 μM aqueous solutions of Cd_4α–MT and Cd_3β–MT at room temperature (20 °C), Fig. 2. A total of six molar

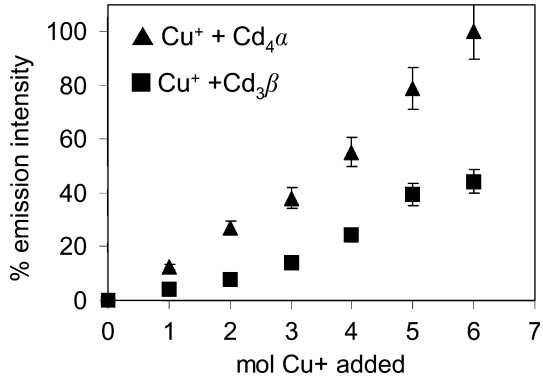

Fig. 2. Relative emission intensity near 600 nm per mole of Cu^+ added to Cd_4α and Cd_3β–MT domains at 20 °C, normalized with respect to the emission of Cu_6α–MT. (The intensity for Cu_6α–MT is set to 100% emission intensity.)

equivalents of Cu^+ were added to each domain and Fig. 2 shows that the relative change in emission intensity per mole of Cu^+ added depends on the Cu:MT ratio but follows a nonlinear trend for both the α and β domains. As the number of copper–thiolate bonds increases during the titration of Cu^+ into the Cd-containing α and β domains, the emission intensity would be expected to increase linearly as a function of moles of Cu^+, however, initially, we observe a nonlinear behavior past the addition of 3 Cu^+ ions up to saturation at 6 Cu^+ ions per domain. We interpret these results as follows: as Cu^+ ions are added to the domain cluster defined by the tetrahedrally coordinating Cd^{2+} ions (as CdS_4) we anticipate that structural changes take place to accommodate the trigonally coordinated Cu^+ ions (as CuS_3). The resultant changes will include both expansion and contraction of the cluster volume. Such changes can cause the protein to become more or less accessible, respectively, to the surrounding solvent and allow for solvent intrusion into the metal binding sites of the protein. Solvent intrusion will deactivate the long-lived 600 nm excited state resulting in lower emission intensities at these stages of the Cu^+ binding reaction. Therefore, we correlate the low quantum yield of intensity in the early stages of the titration to expansion of the cluster, at this stage mixed Cu,Cd-binding exists. As the copper loading increases, we correlate the steeper dependence of the emission intensity with the formation of more compact Cu_6S_{11}-α and Cu_6S_9-β-cluster structures [11]. These conclusions are in agreement with the linear behavior that has been described for the Cu^+ titrations to the metal-free, apo-α, and apo-β domains under low pH conditions [32], where the peptide will form only the copper–thiolate structures so a single coordination environment is expected from $n = 1$ to 6 Cu^+.

The change in emission intensity per mole of Cu^+ added, as shown, is normalized to the quantum yield of emission intensity for the filled Cu_6-cluster; since each domain binds a maximum of 6 Cu^+ ions [14]. From Fig. 2 we can compare the relative quantum yields for each $Cu_n\alpha$ or $Cu_n\beta$-cluster ($n = 0$–6) or the differences between a $Cu_n\alpha$-cluster and a $Cu_n\beta$-cluster. For example, the emission intensity of a $Cu_4\alpha$-cluster is about 67% the emission intensity of a $Cu_6\alpha$-cluster, but a $Cu_4\beta$-cluster is only about 75% the emission of a $Cu_6\beta$-cluster. Overall, the emission intensity observed for any $Cu_n\beta$-cluster is approximately 45% the emission intensity of a $Cu_n\alpha$-cluster. These data show that generally, the $Cu_n\beta$-clusters are much less emissive than $Cu_n\alpha$-clusters. While it has been previously proposed that the copper–thiolate clusters in the α domain of mammalian MT emit more strongly than those in the β domain [33,34], this is the first direct proof of the emissive differences between the two domains of MT made under identical conditions and for metal-replacement reactions that likely take place in the cell. This difference in relative quantum yield leads us to conclude that the $Cu_6\beta$-cluster must have a more porous structure than the $Cu_6\alpha$-cluster, to provide greater solvent accessibility, and therefore lower quantum yields, a property that has been predicted in the proposed Cu_6S_9-β structure in Fig. 1 (bottom). The emission intensity differences that exist between the two domains and between each Cu_n-cluster provide a structure-dependent property that can be correlated to the copper composition of a $Cu_n\alpha$ or $Cu_n\beta$-cluster being formed.

λ_{max} of the emission recorded during cluster building in each copper–thiolate cluster: a probe for the location of copper ions

λ_{max} was determined using the Simpfit program for each emission spectrum recorded as a function of copper loading for μL aliquots of Cu^+ added to 10 μM aqueous solutions of $Cd_4\alpha$–MT and $Cd_3\beta$–MT at room temperature (20 °C). Fig. 3 shows the change in λ_{max} per mole of Cu^+ added to each domain. λ_{max} shifts from 594.5 to 600.5 nm for Cu^+ bound to the β domain of MT, up to the filled $Cu_6\beta$–MT cluster, and λ_{max} shifts from 603.5 to 606.5 nm for Cu^+ bound to the α domain of MT, up to the filled $Cu_6\alpha$–MT cluster. The observed difference in λ_{max} between the α and β domains can arise from the differences in the structures of the copper–thiolate clusters formed in each domain (the structures shown in Fig. 1 are quite different in the environment for each copper). In Fig. 3, initially, the 1–2 mol Cu^+ additions exhibit only a small change in λ_{max}, for 3 and 4 mol Cu^+, there is a significant change in λ_{max}, and the value of λ_{max} levels off between 4 and 6 Cu^+.

This trend in λ_{max} can be explained in terms of the environment of the Cu^+ at different stages of the titration. Initially, the Cu^+ is binding to a cluster formed

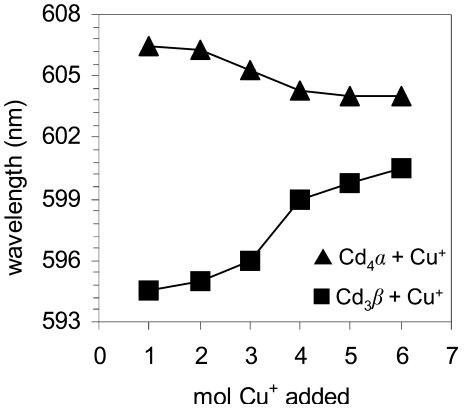

Fig. 3. Band maxima per mole of Cu^+ added to $Cd_4\alpha$ and $Cd_3\beta$–MT domains at 20 °C. Band maxima values were obtained by fitting the emission spectra measured from 400 to 800 nm with Simpfit [37].

from tetrahedral Cd^{2+} ions. The Cd_3S_9 (β-cluster) and Cd_4S_{11} (α-cluster) dominate the stereochemistry of the incoming Cu^+ (Fig. 1, top). With 2 or more Cu^+ added, trigonal coordination for CuS_3 structures will form that involve Cu–S–Cu bridging [2,4]. Therefore, the change in λ_{max} can be correlated to the change in sulfur binding from terminal (Cu–S) and/or mixed Cu,Cd to the bridging (Cu–S–Cu) expected for the higher copper loading stage in the filling of each cluster (Fig. 1). This change in λ_{max} is more pronounced in the β domain, most likely due to its lower content of cysteinyl sulfurs, and therefore and higher content of bridging sulfurs (Fig. 1). Consequently, the λ_{max} differences that exist between the two domains provide a sensitive structure-dependent property that can be correlated to the location of copper ions as either in the α or the β domain of MT. Together, the emission intensity and λ_{max} become parameters with which to monitor the distribution of Cu^+ ions between the α and β domains of metallothionein as a function of time when both domains are present.

In experiments using metal free domains it has been reported that the emission of Cu_6β–MT occurs at 595 nm and is centered near 615 nm for Cu_6α–MT (uncorrected values) [32]. While the two domains exhibit the same trend as we have reported, we suggest that the differences in absolute value arise from the use of metal-free peptides compared with the Cd-containing domains used in this study.

Domain mixing experiments: kinetics of reactions between $Cu_6\alpha$ and $Cd_3\beta$–MT and $Cu_6\beta$ and $Cd_4\alpha$–MT

In the first spectroscopic study specifically of the rate of Cu^+ binding to mammalian Zn_7–MT, a model was proposed that involved the incoming Cu^+ to rearrange from a kinetically controlled distributed product to a thermodynamically controlled domain-specific product over a period of 20 min [33]. The proposed mechanism involved initial binding of Cu^+ ions to both the α and β domains of Zn_7–MT in a noncooperative, random manner, followed by a rearrangement of the Cu^+ ions from the α domain to fill the β domain [34,38]. Proteolytic studies using rat liver MT have shown that Cd^{2+} and Zn^{2+} have a preference for binding to the α domain, whereas Cu^+ binds preferentially to the β domain. However, other than reports of the preferential binding of Cu^+ to the β domain [14,16–21,26,27], no direct evidence in support of a rearrangement has ever been reported. There are no reports that suggest how the distribution might take place in vivo where metallation of both domains will occur on a kinetic basis. No reports exist that demonstrate active transfer of copper from one domain to the other, a mechanism required if the kinetic model described above is appropriate.

Cu^+ migration from the α to the β domain can be detected by changes in emission intensity

Fig. 4 trace A shows the change in emission intensity near 600 nm when Cd_3β–MT is mixed in a single, equimolar aliquot to a solution of Cu_6α–MT. A steep decrease in intensity in the first 100 s is observed, with the intensity reaching a plateau at $I_\infty = 33\%$ after 1000 s. If no migration of Cu^+ ions occurred from the Cu_6α–MT to the Cd_3β–MT, no change in emission intensity for the Cu_6α–MT species would be observed. The rapid and continuing decrease in emission intensity with time clearly can be correlated with migration of Cu^+ ions from the α domain to the less emissive β domain, based on the calibration data provided in Fig. 2. The reaction data were best fitted with a double exponential decay function, indicating a reaction process that requires more than one step. The fitted parameters include a rapid Cu^+ transfer rate of $\sim 2 \times 10^{-1}\,s^{-1}$ and a slower rate of $\sim 8 \times 10^{-3}\,s^{-1}$. The faster rate indicates an immediate transfer of Cu^+ ions from the α to the β domain, a kinetically driven process, while the second rate can be correlated with the redistribution of Cu^+ ions within the new cluster, a thermodynamically driven process. The steps of this reaction model the process seen in Cu^+ binding to the two domain rabbit liver Zn_7–MT2a [38,39], providing direct evidence for the first time of Cu^+ transfer and domain–domain interactions in the two-domain mammalian metallothioneins. These results still leave open the extent of Cu^+ transfer. Figs. 5 and 6

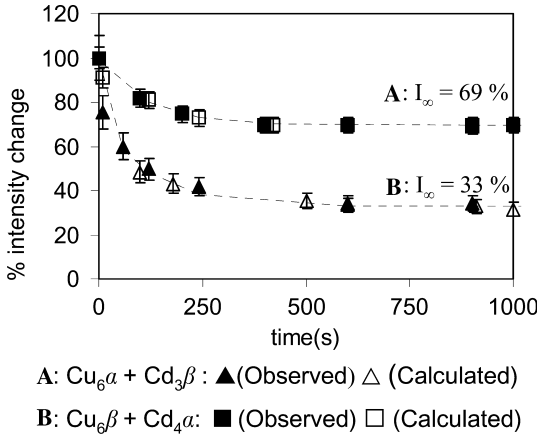

Fig. 4. Observed and predicted (calculated) changes in emission intensity near 600 nm monitored over a period of 1000 s at 20 °C, following mixing of (A) equal volumes of a 10 μM solution of Cu_6α and a 10 μM solution of Cd_3β–MT, (B) equal volumes of a 10 μM solution of Cu_6β and a 10 μM solution of Cd_4α–MT. The emission intensities of the mixing products have been normalized to represent the percentage change from the initial emission intensity found at $t = 0$ s. Emission intensities have also been volume corrected to account for the dilution of the starting emissive solution that occurs when mixing. (The calculated intensities are based on the copper distributions between the two domains described in fourth subsection of Results and discussion and Fig. 6. The copper-distribution model uses the intensity and wavelength data in Figs. 2 and 3 as data in the calculation.)

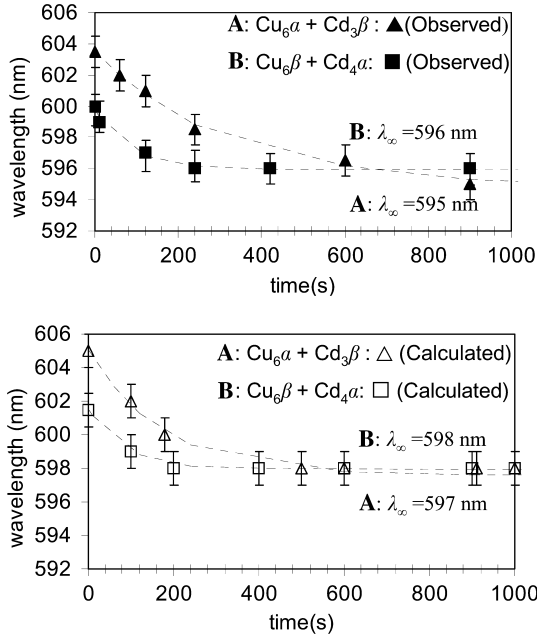

Fig. 5. Change in λ_{max} for the copper–thiolate cluster emission spectra for the mixing experiments monitored over a period of 1000 s. (top) observed, (bottom) calculated. (Calculated λ_{max} are based on the copper distributions between the two domains described in fourth subsection of Results and discussion and Fig. 6. The copper-distribution model uses the intensity and wavelength data in Figs. 2 and 3 as data in the calculation.) (A) λ_{max} change when mixing equimolar volumes of $Cu_6\alpha$ and $Cd_3\beta$–MT. (B) λ_{max} change when mixing equimolar volumes of $Cu_6\beta$ and $Cd_4\alpha$–MT. (λ_{max} values were obtained by fitting the emission spectral data with Gaussian bands using the program Simpfit [37]).

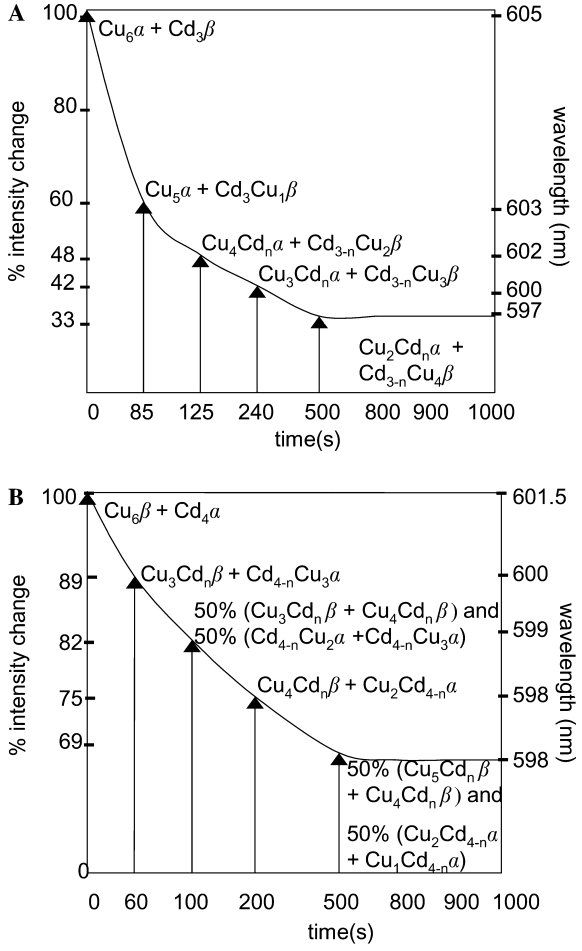

Fig. 6. Calculated Cu and Cd distribution in the mixed α and β-MT species found at several time intervals during the mixing experiments described in Figs. 4 and 5. The compositions were determined by calculating the λ_{max} and emission intensity for all possible compositions that would yield a minimal difference between the observed data in Figs. 4 and 5 by using data shown in Fig. 2 and 3. Species found in solution are 100% unless otherwise stated. (The time in the *x*-axis is not to scale.)

discussed below provide more data to support this model.

Fig. 4 trace B shows how the addition of an equimolar aliquot of $Cd_4\alpha$–MT to $Cu_6\beta$–MT results in a much slower decline in emission intensity as a function of time, to $I_\infty = 69\%$ at 1000 s. The final emissive species in Fig. 4 trace B exhibits roughly 2.1× greater emission intensity when compared to that observed in Fig. 4 trace A, a difference we propose is due to the migration of Cu^+ from the less emissive β domain to the more emissive α domain. The kinetic data were fitted to a single exponential decay function describing a single step reaction process with a rate of $\sim 8 \times 10^{-3}\ s^{-1}$. It has been shown previously that following mixing of Zn_7–MT and Cd_7–MT there is a slow metal redistribution process between the domains as formation of thermodynamically stable, mixed-metal products takes place [30]. Therefore, in this scenario we correlate the distribution of Cu^+ from the β to the α domain to be a similar process, in which the thermodynamically stable, mixed metal Cd,Cu-β and Cd,Cu-α products form. The differences that arise between the two scenarios suggest a greater extent of Cu^+ transfer from the α domain to the β domain, due to the greater change in intensity. The calculated data points shown in Fig. 4 represent the sum of the intensities of the species present at that point in time using data in Figs. 2 and 3 to allow determination of the copper-loading in each domain. Again, data in Figs. 5 and 6 provide more data to support this model and it will be further discussed in fourth subsection of Results and discussion.

Cu^+ migration from the α to the β domain detected by changes in λ_{max}

The time dependence of the change in λ_{max} values was extracted from the spectral data recorded during the mixing experiments through the use of the band-fitting program Simpfit, and the results are shown in Fig. 5. Fig. 5 (top) trace A shows that λ_{max} shifts from 603.5 to 595.0 nm following the mixing of $Cu_6\alpha$–MT with $Cd_3\beta$–MT over a period of 1000 s. These kinetic data were fitted by a double exponential decay function to give

rates of $\sim 5 \times 10^{-3}$ nm/s and $\sim 4 \times 10^{-3}$ nm/s, describing a reaction process that requires more than one step, as previously described for the same reaction process taking place in Fig. 4 trace A, but followed by the change in relative emission intensity. Fig. 5 (top) trace B shows that λ_{max} changes from of 600.5 to 596.0 nm following mixing of $Cu_6\beta$–MT with $Cd_4\alpha$–MT. This change takes place with a single exponential decay rate of $\sim 1 \times 10^{-2}$ nm/s describing a single step reaction process, matching the change in emission intensity taking place in Fig. 4 trace B.

Significantly, these data clearly show that neither reaction forms the fully metallated Cu_6-cluster at t_∞ since the wavelengths of the final products do not match the wavelength of the associated Cu_6-cluster (600.5 nm for a $Cu_6\beta$-cluster and 603.5 nm for a $Cu_6\alpha$-cluster) shown in Fig. 3. Therefore, taken together, the changes in emission intensity and the changes in λ_{max} that take place as $Cu_6\alpha$–MT is mixed with $Cd_3\beta$–MT and $Cu_6\beta$–MT is mixed with $Cd_4\alpha$–MT allow us to conclude that mixed metal Cd,Cu-species are formed. These Cd,Cu-species have unique metal stoichiometries that result in independent emission intensities and λ_{max} values at t_∞ following mixing.

The data also show that the extent of Cu^+ distribution observed for the mixing of $Cu_6\beta$–MT with $Cd_4\alpha$–MT and $Cu_6\alpha$–MT with $Cd_3\beta$–MT is very different, there is a greater shift in λ_{max} when $Cu_6\alpha$–MT is mixed with $Cd_3\beta$–MT, indicating that there is a greater extent of Cu^+ transfer to the β domain as shown in Fig. 4. So, we conclude that there is preferential binding of Cu^+ to the β domain. Shifts in λ_{max} have also been reported for Cu^+ binding to the metal-free, apo(βα)MT, individual domains, and mixed isolated domains of MT [32], but with inconclusive results. The shift in λ_{max} observed for the mixed domain fragments with Cu^+ was not explained. However, the data presented here allow interpretation of these results in terms of competition between each domain for the Cu^+ ions that are added. This competition changes as the number of copper atoms bound to either of the domains increases, so that for the mixtures of β and α MT fragments, both domains compete to bind Cu^+ to varying extents over the course of the reaction making it difficult to determine specific domain loading λ_{max} values until the maximum number of copper atoms has been added, which is 12, ending in $Cu_6\alpha$–MT and $Cu_6\beta$–MT with its specific λ_{max} value.

It has long been proposed that Cu^+ preferentially binds to the β domain of metallothionein and many studies since then have supported this idea [14,16–21,26,27] but we have taken advantage of the emissive differences (intensity and band maxima, λ_{max}) that exist between the two domains of MT to monitor the preferential binding of Cu^+ to the β domain of MT as a function of time in the presence of both domains of MT and Cu^+. However, we still need to know if the copper binding sites in both domains fill with a similar mechanism, and most importantly what is the mechanism of copper binding to MT for the formation of $Cu_6\alpha$ and $Cu_6\beta$–MT clusters?

Simulations to determine the Cu and Cd compositions in the individual domains of MT on their way to the formation of $Cu_6\alpha$ and $Cu_6\beta$–MT clusters based on emission intensity and λ_{max} data

Addition of Cu^+ to $Cd_3\beta$–MT and $Cd_4\alpha$–MT results in Cu,Cd mixtures that exhibit unique emission spectral parameters, defined by specific emission intensities (which are related to the quantum yields) and band maxima (λ_{max} values), Figs. 2 and 3. In this part of the study, extensive simulations were carried out by combining the specific emission intensity and λ_{max} values (obtained from Simpfit) for a wide range of Cd,Cu_n-α and/or Cd,Cu_n-β cluster combinations that could yield the particular emission intensity and band maxima observed over time during the mixing experiments. By using these calculated data, the intensity profiles in Fig. 4 and the wavelength profiles in Fig. 5 have been simulated with specific Cd and Cu-α and β metallated species. The predicted experimental data for these compositions are superimposed on the experimental data in Figs. 4A and B and shown separately in Fig. 5 (bottom), and these are referred to as the calculated data. These simulations allowed for identification of the Cu and Cd compositions that exist in the α and β domains of MT at specific time intervals during the mixing experiments.

Fig. 6 summarizes the change in Cd,Cu composition in the α and β domains of MT as a function of time following the mixing of $Cu_6\beta$–MT with $Cd_4\alpha$–MT and $Cu_6\alpha$–MT with $Cd_3\beta$–MT, based on the calculated spectra shown in Figs. 4 and 5. According to the sequence of compositions shown in Fig. 6, the emission intensity profiles in Fig. 4 are fitted extremely well. The close correspondence between these two sets of data allows us to determine the exact Cd,Cu-domain species that are formed in solution at each time interval. In Fig. 6A, we show how mixing $Cu_6\alpha$–MT with $Cd_3\beta$–MT results in the rapid decline in emission intensity that is connected with a reduction in λ_{max} so that at 1000 s the final product of the mixing reaction described in Figs. 4 trace A and 5 (top) trace A is identified as a mixture of $Cd_{3-n}Cu_4\beta$–MT and $Cu_2Cd_n\alpha$–MT. In Fig. 6B, we show how mixing $Cu_6\beta$–MT with $Cd_4\alpha$–MT results in the slower decline of emission intensity that is connected with a slower reduction in λ_{max} so that at 1000 s the final product of the mixing reaction described in Figs. 4B and 5 (top) trace B is identified as a mixture of $Cu_{4-5}Cd_n\alpha$–MT and $Cu_{1-2}Cd_{4-n}\beta$–MT.

According to the simulated spectral data (emission intensities and λ_{max}) shown in Fig. 6, only a few cluster compositions are possible. The $Cu_4\beta$-cluster is prominent in both mixing experiments. This strongly suggests that the $Cu_4\beta$-cluster could be a possible intermediate required for the formation of the $Cu_6\beta$-cluster in the presence of low copper concentrations. We can also conclude that Cu^+ preferentially binds to the β domain due to the higher Cu^+ stoichiometry found in that domain by the end of each mixing experiment. The presence of a Cu_4-cluster intermediate in the β domain has been identified from previous copper binding studies of Zn_7–MT [26–28], but it has not been previously linked to the Cu^+ exchange phenomena between the α and β domain. This observation supports the idea that a $(Cu_6\alpha)(Cu_6\beta)$–MT species would be unlikely in vivo under conditions of low Cu^+ concentrations because native Zn_7–MT synthesized by mammals fed or injected with metals such as Cu^+ always yielded mixed-metal clusters that contained Zn^{2+} ions [6,10,40,41]. Mass spectrometry studies of Cu^+ binding to Zn_7- and Cd_7–MT have shown the presence of mixed-metal species [26–28], but no stoichiometric distribution of Cu^+ between the α and β domains of MT could be observed as a function of time as it has been possible in this paper.

Conclusion

This paper has shown how the copper–thiolate specified emission of Cu–MT is dependent on the Cu:MT ratio. The emission intensity follows a nonlinear relationship due to the disturbance of CuS_3 bonds by slight exposure to the solvent during periods of expansion by the polypeptide to allow for Cd^{2+} displacement by Cu^+. The $Cu_n\beta$-cluster of MT was found to be 2.2× less emissive than the Cuα-cluster, and, therefore, the copper–thiolate specified emission is shown to be dependent on the domain-location of the Cu^+ ions. Wavelength data also provide a separate and concentration independent tool with which to study the location of Cu^+ within the domains of MT in vivo, because it solely depends on copper loading. Both the emission intensity and λ_{max} are properties determined by the specific structure adopted by the copper–thiolate cluster in each domain.

Specific emission intensity and the λ_{max} values of each domain were shown to be useful in monitoring the preferential binding of Cu^+ towards the β domain of MT. Furthermore, the specific emissive characteristics of each $Cu_n\alpha$ and $Cu_n\beta$-cluster were used to monitor a unique pathway for the formation of Cu_6S_{11} and Cu_6S_9-clusters in the α and β domains of $M_7(\beta\alpha)$–MT respectively. This pathway requires Cu^+ exchange reactions between the two domains, which involve the migration of Cu^+ from the α to the β domain of MT, followed by formation of a Cu_4-cluster intermediate localized in the β domain of MT before any Cu^+ ions remain bound to the α domain. The Cu_4-β-cluster intermediate is identified as a major intermediate species in the copper binding reactions and might be a key intermediate in the formation of $Cu_6\alpha$ and $Cu_6\beta$–MT species.

Acknowledgments

The authors thank past and present group members for their help in many aspects of the work described here, and the collaboration of Dr. Peter Kille at Cardiff, UK. We thank Dr. John Mack for assistance with Simpfit. We acknowledge financial support from NSERC in the form of equipment and operating funds (to M.J.S.), and financial support by the Ontario Graduate Scholarship in Science and Technology (to M.T.S.) and the Academic Development Fund at UWO (to M.J.S.).

References

[1] (a) T.O. Scholl, T.M. Reilly, in: J. Bogden, L.M. Klevay (Eds.), Clinical Nutrition of the Essential Trace Elements and Minerals, Humana Press, New Jersey, 2000, pp. 289–307;
(b) J.F. Mercer, D. Kramer, J. Camakaris, in: E.J. Massaro (Ed.), Handbook of Copper Pharmacology and Toxicology, Humana Press, New Jersey, 2002, pp. 249–276;
(c) B. Sarkar, J. Inorg. Biochem. 79 (2000) 187–191;
(d) A. Mas, B. Sarkar, Handbook of Metal–Ligand Interactions in Biological Fluids Bioinorganic Chemistry, vol. 2, 1995, pp. 784–788.
[2] C.D. Klaasen (Ed.), Metallothionein IV, Birkhauser Verlag, Basel, 1999, pp. 23–45, see also pp. 397–401.
[3] (a) P.J. Aggett, S.M. Barclay, in: R.M. Cowett (Ed.), Principles of Perinatal–Neonatal Metabolism, Neonatal Trace Element Metabolism, Springer-Verlag, Berlin, 1991, pp. 500–530;
(b) D.H. Petering, B.A. Fowler, Environ. Health Perspecti. 65 (1986) 217–224.
[4] (a)J.H.R. Kagi, Y. Kojima (Eds.), Metallothionein II. Exp. Sup. 52, Birkhauser Verlag, Basel, Switzerland, 1987;
(b) M.J. Stillman, C.F. Shaw III, K.T. Suzuki (Eds.), Metallothioneins, VCH Publishers, New York, 1992;
(c) D.T. Suzuki, N. Imura, M. Kimura (Eds.), Metallothionein III, Birkhauser Verlag, Basel, 1993.
[5] K.S. Squibb, R.J. Cousins, S.L. Feldman, Biochem. J. 164 (1977) 223–228.
[6] I. Bremner, B.W. Young, Biochem. J. 157 (1976) 517–520.
[7] R.D. Andersen, W.P. Winter, J.J. Maher, I.A. Bernstein, Biochem. J. 174 (1978) 327–338.
[8] S. Ohi, G. Cardenosa, R. Pine, P.C. Huang, J. Biol. Chem. 256 (1981) 2180–2184.
[9] D.M. Durnam, R.D. Palmiter, J. Biol. Chem. 256 (1981) 5712–5716.
[10] J.D. Otvos, I.M. Armitage, Proc. Natl. Acad. Sci. USA 77 (1980) 7094–7098.
[11] A. Presta, D.A. Fowle, M.J. Stillman, J. Chem. Soc., Dalton Trans. (1997) 977–984.
[12] Y. Boulanger, I.M. Armitage, J. Inorg. Biochem. 17 (1982) 147–153.
[13] D. Fowle, M.J. Stillman, J. Biomol. Struct. Dyn. 14 (1997) 393–406.
[14] K.B. Nielson, D.R. Winge, J. Biol. Chem. 259 (1984) 4941–4946.
[15] D.R. Winge, C.T. Dameron, in: K.T. Suzuki, N. Imura, M. Kimura (Eds.), Metallothionein II, Birkhauser Verlag, Basel, 1993, pp. 381–397.

[16] (a) J.D. Otvos, I.M. Armitage, in: B.D. Sykes, J. Glickson, A.A. Bothnerby (Eds.), Biochemical Structure Determination by NMR, Marcel Dekker, New York, 1982, pp. 65–96;
(b) I.M. Armitage, J.D. Otvos, R.W. Briggs, Y. Boulanger, Fed. Proc. 41 (1982) 2974–2980.
[17] K.B. Nielson, D.R. Winge, J. Biol. Chem. 258 (1983) 13063–13069.
[18] F. Vazquez, M. Vasak, Biochemistry J 253 (1988) 611–614.
[19] I.M. Armitage, Y. Boulanger, in: P. Lazlo (Ed.), NMR of Newly Accessible Nuclei, vol. 2, Academic Press, New York, 1983, pp. 337–365.
[20] K.B. Nielson, D.R. Winge, J. Biol. Chem. 260 (1985) 8698–8701.
[21] P. Chen, A. Munoz, D. Netteshein, C.F. Shaw III, D.H. Petering, Biochem. J. 317 (1996) 395–402.
[22] A. Presta, A.R. Green, A. Zelazowski, M.J. Stillman, Eur. J. Biochem. 227 (1995) 226–240.
[23] M.J. Stillman, A. Presta, Z. Gui, D. Jiang, Metal Base Drugs 1 (1994) 375–394.
[24] M.J. Stillman, Z. Gasyna, in: B. Vallee, J.F. Riordan (Eds.), Methods in Enzymology, Metallobiochemistry Part B, Metallothionein and Related Molecules, vol. 205, Academic Press, New York, 1991, p. 540.
[25] M.J. Stillman, Coord. Chem. Rev. 144 (1995) 46.
[26] R. Bofill, M. Capdevila, N. Cols, S. Atrian, P. Gonzalez-Duarte, J. Biol. Inorg. Chem. 6 (2001) 405–417.
[27] L.T. Jensen, J.M. Peltier, D.R. Winge, J. Biol. Inorg. Chem. 3 (1998) 627–631.
[28] F. Roschitzki, M. Vasak, J. Biol. Inorg. Chem. 7 (2002) 611–616.
[29] K.B. Nielson, C.L. Atkin, D.R. Winge, J. Biol. Chem. 260 (1985) 5342–5350.
[30] M.J. Stillman, W. Cai, A.J. Zelazowski, J. Biol. Chem. 262 (1987) 4538–4548.
[31] M.J. Stillman, A.J. Zelazowski, J. Biol. Chem. 263 (1988) 6128–6133.
[32] Y.J. Li, U. Weser, Inorg. Chem. 31 (1992) 5526–5533.
[33] A.R. Green, A. Presta, Z. Gazyna, M.J. Stillman, Inorg. Chem. 33 (1994) 4159–4168.
[34] A.R. Green, M.J. Stillman, Inorg. Chem. 35 (1996) 2799–2807.
[35] M.E. Merrifield, Z. Huang, P. Kille, M.J. Stillman, J. Inorg. Biochem. 88 (2002) 153–172.
[36] (a) G.L. Ellman, Arch. Biochem. Biophys. 8 (1959) 70–77;
(b) W. Birchmeier, P. Christen, FEBS Lett. 18 (1971) 209–213.
[37] (a) Z. Gasyna, W.R. Browett, T. Nyokong, R. Kitchenham, M.J. Stillman, Chemometr. Intell. Lab. Syst. 5 (1989) 233;
(b) J. Mack, W.R. Browett, M.J. Stillman, 2004, submitted for publication.
[38] J. Chan, Z. Huang, M.E. Merrifield, M.T. Salgado, M.J. Stillman, Coord. Chem. Rev. 233-234 (2002) 319–339.
[39] M.J. Stillman, D. Thomas, C. Trevithick, X. Guo, M. Siu, J. Inorg. Biochem. 79 (2000) 11–19.
[40] I. Bremmer, B. Young, Biochem. J. 155 (1976) 631–635.
[41] R.W. Briggs, I.M. Armitage, J. Biol. Chem. 257 (1982) 1259–1262.